Short communication

A radiotracer study of the adsorption behavior of aqueous Ba^{2+} ions on nanoparticles of zero-valent iron

O. Çelebi [a], Ç. Üzüm [b], T. Shahwan [b,*], H.N. Erten [a]

[a] *Department of Chemistry, Bilkent University, 06800 Bilkent, Ankara, Turkey*
[b] *Department of Chemistry, İzmir Institute of Technology, 35430 Urla, İzmir, Turkey*

Abstract

Recently, iron nanoparticles are increasingly being tested as adsorbents for various types of organic and inorganic pollutants. In this study, nanoparticles of zero-valent iron (NZVI) synthesized under atmospheric conditions were employed for the removal of Ba^{2+} ions in a concentration range 10^{-3} to 10^{-6} M. Throughout the study, ^{133}Ba was used as a tracer to study the effects of time, concentration, and temperature. The obtained data was analyzed using various kinetic models and adsorption isotherms. Pseudo-second-order kinetics and Dubinin–Radushkevich isotherm model provided the best correlation with the obtained data. Observed thermodynamic parameters showed that the process is exothermic and hence enthalpy-driven.
© 2007 Elsevier B.V. All rights reserved.

Keywords: Nano-zero-valent iron; Barium; Adsorption

1. Introduction

Zero-valent iron (ZVI) was proposed as a reactive material in permeable reactive barriers (PRGs) due to its great ability in reducing and stabilizing different types of pollutants [1]. During the last years, there has been an increasing interest in synthesizing this material on nanoscale in order to enhance its remediation ability by virtue of the increase in the surface area and surface reactivity of the particles [2]. It was reported that the rates of adsorption of Cr(IV) and Pb(II) increased by 30 times for NZVI in comparison to iron fillings or iron powder (325 mesh) [3].

Literature resources contain plenty of works in which NZVI was applied for the removal of various organic materials (e.g. [4–6]). Comparatively, less effort was devoted to studying the adsorption of metal ions on NZVI. The ions investigated so far include As(III) and As(V) [7–9], Pb(II) [3], Cr(VI) [10], Ni(II) [11], and other ions [12]. No reports are present on the applicability of NZVI for radioactive isotopes which are important from radioactive waste management viewpoint.

Barium, Ba, is an alkaline earth element ($Z = 56$), the compounds of which are used in various industries like paint, glass, ceramics, and as an oil additive. This element possesses also a large number of radioactive isotopes, but the most important ones are ^{133}Ba ($t_{1/2} = 10.7$ year) which has a relatively long half life, and ^{140}Ba ($t_{1/2} = 12.79$ day) which is a fission product produced in a high yield. In addition, Ba is an ideal analogue of Ra as both occur in the same group and possess close ionic radii (Ba^{2+} = 1.34 Å, Ra^{2+} = 1.43 Å) [13]. Thus assessing the behavior of Ba will be helpful also in predicting that of Ra, an element with several radioisotopes that are important in radioactive waste considerations, has a high mobility in the geosphere, and thus high accessibility to the food chain.

NZVI used in this study was synthesized by liquid-phase reduction under open atmosphere. The purpose of this work was to assess the effects of time, concentration, adsorbent dose, and temperature on the extent of Ba^{2+} retention by NZVI. The obtained experimental data were described using various kinetic and isotherm models, and the thermodynamic parameters associated with the adsorption process were calculated. The activity of Ba^{2+} samples prior to and following adsorption was determined using γ-ray spectro scopy. The adsorbent was characterized by X-ray diffraction (XRD), and scanning electron microscopy/energy dispersive X-ray spectroscopy (SEM/EDS).

---

* Corresponding author. Fax: +90 232 750 7509.
E-mail address: talalshahwan@iyte.edu.tr (T. Shahwan).

2. Experimental

2.1. Preparation of NZVI

NZVI used in this study was synthesized using the method of liquid-phase reduction also known as the borohydride method. The procedure followed is primarily based on a previously reported method [14]. In each batch, a sample of $FeCl_2 \cdot 4H_2O$ weighing 17.8 g was dissolved in 50 ml of absolute ethanol and distilled water solution (4:1 v/v). As the reducing agent, 8.47 g $NaBH_4$ was dissolved in 220 ml of distilled water to have ∼1 M solution. The $NaBH_4$ solution was added to Fe^{2+} solution at rate of 40–50 drops/min, while well stirring the reaction mixture. The resulting reaction can be given as

$$Fe^{2+} + 2BH_4^- + 6H_2O \rightarrow Fe^0 + 2B(OH)_3 + 7H_2\uparrow$$

Black particles of NZVI appeared immediately after introducing the first drops of $NaBH_4$ solution. Further mixing for 20 min was allowed following the addition of $NaBH_4$ solution. The iron powder was separated from the solution using vacuum filtration. The filtrate was then washed at least three times with 99% absolute ethanol. This washing step appeared to be critical in stabilizing NZVI against immediate oxidation, as samples washed with deionized water showed much faster oxidation. This is in line with previous reports on the topic [4,14]. Finally, the powder was taken into a watch glass and dried at 75 °C overnight in an oven without air evacuation. It was observed that drying under vacuum caused the samples to rapidly catch fire upon exposure to atmospheric oxygen.

2.2. Adsorption experiments

Throughout this study, batch experiments were conducted with ^{133}Ba ($t_{1/2} = 10.7$ year) applied as the radioactive tracer. About 400 μl of the radionuclide solution were added to a 1 L solution of Ba^{2+} (prepared from $BaCl_2$ salt). The initial count rates were measured for 4.0 ml aliquots of barium solutions using the γ-ray peak at 361 keV, and were above 50 000 cps/ml in all cases.

In order to check any loss in activity originating from adsorption onto the inside surface of tubes used in the experiments, blank experiments were performed using solutions without the adsorbent material. The results showed that adsorption onto tube surface were negligible. During the adsorption experiments lateral shaking was performed in a temperature-controlled environment using a Nuve ST 402 water bath shaker equipped with microprocessor thermostat, with the tubes being horizontally oriented to ensure efficient mixing. The fluctuation in controlled temperature was less than ±1.0 °C.

The kinetic experiments were performed by adding 10 ml of aliquots of the radioactive Ba^{2+} solution (1×10^{-4} M) to 100 mg samples of iron nanoparticles. The mixtures were shaken at room temperature for periods ranging from 5 min to 24 h. The resulting solutions were centrifuged and 4 ml portions of the liquid phases were counted to determine their activities.

The loading experiments included the initial Ba^{2+} concentrations of 1×10^{-3}, 5×10^{-4}, 1×10^{-4}, 1×10^{-5}, and 1×10^{-6} M. These investigations were performed by contacting 10 ml of aliquots of the radioactive Ba^{2+} solution with 100 mg samples of iron nanoparticles at two different temperatures, 25 and 55 °C. In order to examine the effect of the applied amount of iron nanoparticles on the extent of adsorption, further experiments were conducted at 25 °C using 50 and 25 mg samples. The mixtures were shaken for 5 h, centrifuged, and 4 ml of portions of the liquid-phase were counted. The experiments were performed in duplicates, and the average values were used in the corresponding calculations.

2.3. XRD and SEM characterization

XRD technique was used to elucidate the content of the newly synthesized iron nanoparticles and check the changes after the adsorption of Ba^{2+} ions. The XRD patterns were recorded using a Rigaku Miniflex diffractometer that contains a high-power Cu Kα (λ = 1.54 Å) source operating at 30 kV/15 mA.

SEM analysis was done using a Philips XL-30S FEG type instrument. The solid samples were first sprinkled onto adhesive C tapes supported on metallic disks. Images of the sample surfaces were then recorded at different magnifications.

3. Results and discussion

Iron nanoparticles applied in this work consisted mainly of zero-valent iron, characterized by the basic reflection appearing at 2θ of 44.9°, as shown in the XRD diagram in Fig. 1a. Characterization of the samples stored under ambient conditions for 3 months after their production showed that a limited oxidation took place. As was mentioned in the experimental part, this is owed basically to using ethanol as a solvent during synthesis of NZVI. Another explanation for the slow oxidation was reported to stem from the presence of boron together with iron in the outer shell of the iron particles [9,10]. On the other hand, the exposure of NZVI particles to water during the adsorption of aqueous Ba^{2+} ions caused massive oxidation. This
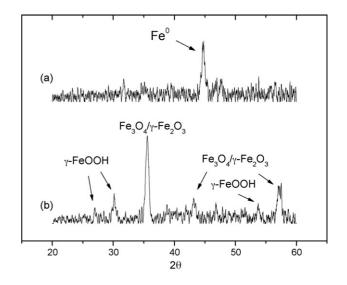

Fig. 1. XRD patterns of iron nanoparticles: (a) before adsorption and (b) after adsorption of Ba^{2+} ions.
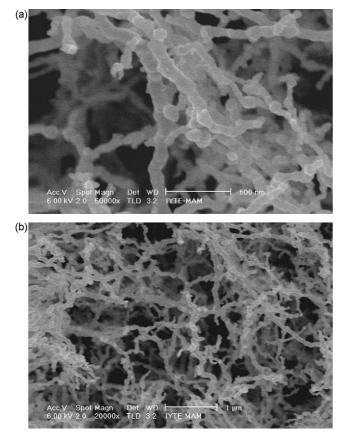
Fig. 2. SEM images of iron obtained at magnification of: (a) 50 000× and (b) 20 000×.

is evident from the XRD diagram in Fig. 1b, where the oxide appear in the form of maghemite (γ-Fe_2O_3), magnetite (Fe_3O_4), and lepidocrocite (γ-FeOOH). The phases of iron oxide, γ-Fe_2O_3 and Fe_3O_4 are indistinguishable by XRD, and thus the corresponding peaks might be standing for either phase or both.

Typical SEM images of a fresh sample of NZVI are demonstrated in Fig. 2. The iron particles appear to possess a size ranging from 20 to 100 nm. These nanoparticles are seen to form chain-like aggregates, demonstrating a morphology that resembles the previously reported ones (e.g. [11,15,16]).

In the following sections, the adsorption data of aqueous Ba^{2+} ions by iron nanoparticles are analyzed from kinetic, equilibrium, and thermodynamics aspects and some comments on the plausible mechanism of adsorption are included.

3.1. Kinetic description

The adsorption of Ba^{2+} on NZVI was first studied at different times of mixing to have an idea about the kinetics of the process. The initial concentration of Ba^{2+} was 0.0001 M, and the solution was contacted with NZVI for time periods that ranged from 5 min up to 24 h. Equilibrium was approached at about 4 h of mixing as shown in Fig. 3. The kinetic findings were described using the Elovich equation [17], Lagergren's equation [18], and the pseudo-second-order model [18,19]. These models are, respectively, given by the following
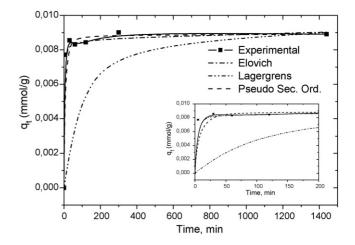

Fig. 3. Variation of the adsorbed amount of Ba^{2+} with time as revealed by the experimental data in comparison to Lagergren's, Elovich, and pseudo-second-order model predictions. The inset figure shows the variation of adsorbed amount at the earlier stage of adsorption.

expressions:

$$q_t = \frac{1}{\beta} \ln(\alpha\beta) + \left(\frac{1}{\beta}\right) \ln t \tag{1}$$

$$q_t = q_e(1 - \exp(-k_1 t)) \tag{2}$$

$$q_t = \frac{k_2 q_e^2 t}{1 + k_2 q_e t} \tag{3}$$

In the above equations, q_t stands for the concentration of Ba^{2+} on the solid at any time, t, and q_e is the equilibrium concentration (mmol/g). k_1 (min^{-1}) and k_2 (g $mmol^{-1}$ min^{-1}) are the rate constants. In Elovich equation, α (mmol g^{-1} min^{-1}) is the initial sorption rate and β (g $mmol^{-1}$) is a parameter related to the extent of surface coverage. The linearized forms of these expressions were used to find the parameters of the models. Table 1 contains the values of these parameters, which were then used to establish the corresponding plots provided in Fig. 3 together with the experimental data. According to the linear correlation

Table 1
Values of the kinetic parameters and linear correlation coefficients (R^2) obtained for Ba^{2+} adsorption on NZVI

Model	Parameter	Value
Lagergren's equation	Slope ± error	$-8.20 \times 10^{-3} \pm 1.74 \times 10^{-3}$
	Intercept ± error	-2.035 ± 0.2574
	k_1 (min^{-1})	0.0082
	R^2	0.8804
Pseudo-second-order equation	Slope ± error	112.01 ± 0.33
	Intercept ± error	251.57 ± 201.17
	k_2 (g/(mmol min))	49.9
	q_e (mmol/g)	0.00893
	R^2	0.9999
Elovich equation	Slope ± error	$2.12 \times 10^{-4} \pm 5.59 \times 10^{-5}$
	Intercept ± error	$7.54 \times 10^{-3} \pm 2.70 \times 10^{-4}$
	α (mmol/(g min))	5.57×10^{11}
	β (g/mmol)	4710
	R^2	0.8847

coefficients, the best description is provided by the pseudo-second-order equation. From Fig. 3, it can also be seen that Elovich equation provided adequate correlation, unlike Lagergren's equation which demonstrated significant deviations, in particular during earlier stages of adsorption.

3.2. Adsorption isotherms

The partition of Ba^{2+} ions at equilibrium between liquid and solid phases was modeled using the adsorption isotherms of Freundlich, Dubinin–Radushkevich (D–R), Temkin, and Langmuir. The equations of these isotherms are, respectively, given by the equations:

$$q_e = kC_e^n \tag{4}$$

$$q_e = q_m \exp(-K\varepsilon^2) \tag{5}$$

$$q_e = \frac{RT}{b}\ln(K_T C_e) = B\ln(K_T C_e) \tag{6}$$

$$q_e = \frac{Kq_m C_e}{1 + KC_e} \tag{7}$$

In the above equation, q_e is as defined above, C_e stands for the equilibrium concentration of Ba^{2+} in solution (mmol/ml). k and n are the Freundlich constants which can be used, respectively, to estimate the sorption affinity and linearity. In D–R model, q_m corresponds to the maximum coverage, K is a constant related to adsorption energy E, which is in turn given by $1/(2K)^{0.5}$. The parameter ε is the Polanyi potential which is equal to $RT\ln[1 + 1/C_e]$. Langmuir constant, K, is related with the heat of adsorption, and q_m corresponds to the monolayer coverage, Temkin constant, B, is connected with the heat of adsorption, and K_T is the equilibrium binding constant (l/g) corresponding to the maximum binding energy [20].

The adsorption data obtained for different doses of NZVI samples were fitted to the linear forms of these equations. The results showed that while Freundlich and D–R isotherms provided proper description of the data, both of Temkin and Langmuir isotherms yielded poor correlations ($R^2 < 0.8000$). The values of the constants of the best fitting models are given in Table 2, and the linear regression plots are shown in Figs. 4 and 5.

The correlation coefficients, which are also included in the same table, suggest that D–R isotherm model provided somewhat better correlation than Freundlich model. It is seen that adsorption proceeds considerably far from linearity as the values of n suggest. Freundlich constant k, which might be viewed as a kind of a distribution coefficient of the adsorbate between solid and liquid phases and thus can be correlated with the capacity of adsorption, showed a decrease with the decreasing amount of NZVI. Within the same range of concentration, a smaller amount of NZVI is expected to relatively adsorb fewer amounts of Ba^{2+} ions, which means a lower adsorption capacity.

The D–R constant, q_m, which is usually conceived as the maximum coverage is seen to increase with the decrease in NZVI amount, probably due to the larger competition associated with the decrease in the available adsorption sites. The E values calculated based on K constants correspond to the amount of energy required to transfer one mole of adsorbate ions from infinity within the solution to the surface of the adsorbent. Minimal increase of E values is seen to parallel the decease in the adsorbent amount.

3.3. Thermodynamic description

The effect of temperature was studied by raising the mixing temperature from 298 to 328 K. At all the studied concentrations, the amounts adsorbed decreased with increasing temperature. The data was used to evaluate the 'observed' thermodynamic parameters; ΔH°, ΔS°, and ΔG° of adsorption. For this purpose, the following relations were used:

$$\log \frac{R_{d2}}{R_{d1}} = -\frac{\Delta H^\circ}{R}\left(\frac{1}{T_2} - \frac{1}{T_1}\right) \tag{8}$$

$$\Delta G^\circ = -RT \ln R_d \tag{9}$$

$$\Delta S^\circ = \frac{\Delta H^\circ - \Delta G^\circ}{T} \tag{10}$$

The thermodynamic parameters are described as 'observed' because they roughly include the contributions from dehydration forces in addition to the contributions of the energy of intrinsic adsorption. The equilibrium partitioning of Ba^{2+} ions between

Table 2
Freundlich and D–R constants obtained at different doses of NZVI applied for Ba^{2+} adsorption

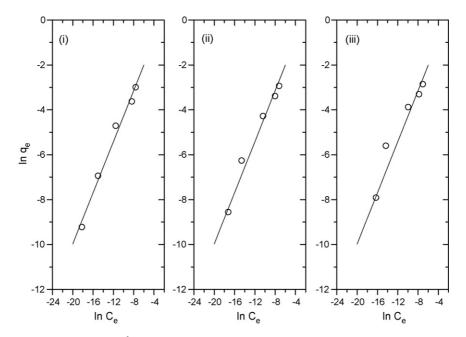| Isotherm model	Parameter	Amount of NZVI		
		100	50	25
Freundlich	Slope ± error	0.5692 ± 0.0402	0.5331 ± 0.0471	0.4947 ± 0.0732
	Intercept ± error	1.4095 ± 0.5134	1.0437 ± 0.5717	0.7724 ± 0.8539
	n	0.5692	0.5331	0.4947
	k	4.0938	2.8397	2.1650
	R^2	0.9853	0.9771	0.9383
D–R	Slope ± error	−0.3641 ± 0.0119	−0.3590 ± 0.0164	−0.3463 ± 0.0401
	Intercept ± error	−1.8512 ± 0.1410	−1.8455 ± 0.1759	−1.8035 ± 0.3974
	q_m (mmol/g)	0.1570	0.1579	0.1647
	K (mol/kJ)^2	0.00364	0.00359	0.00346
	E (kJ/mol)	11.7	11.8	12.0
	R^2	0.9968	0.9938	0.9612

Fig. 4. Freundlich isotherm plots for Ba^{2+} adsorption on NZVI at different adsorbent doses: (i) 100 mg, (ii) 50 mg, and (iii) 25 mg.

liquid and solid phases is expressed in the above equations using the distribution ratio, R_d, given by

$$R_d = \frac{q_e}{C_e} \qquad (11)$$

where q_e and C_e are the equilibrium concentrations on the solid (mmol/g) and in the liquid (mmol/ml), respectively. For adsorption on solids, the energy barrier of adsorption normally increases as loading is increased and hence, the values of q_e and C_e at equilibrium will depend on that of the initial concentration. In such a situation, adsorption will be nonlinear and consequently the obtained R_d values are also a function of the initial

concentration, decreasing as the latter is increased. In this sense, R_d is a phenomenological equilibrium constant, as revealed by Fig. 6 constructed at different amounts of NZVI. Therefore, the calculated thermodynamic parameters are valid for a specific set of conditions, specifically the applied concentration.

The values of the thermodynamic parameters, ΔH°, ΔG° and ΔS° calculated using the above equations are provided in Table 3. The negative sign of ΔH° reflects the exothermic nature of adsorption and show an increase as the initial concentration is decreased. In order to evaluate the enthalpy change at infinite dilution (ΔH_{id}°), the observed ΔH° values were plotted as a function of initial concentration (log scale). When the
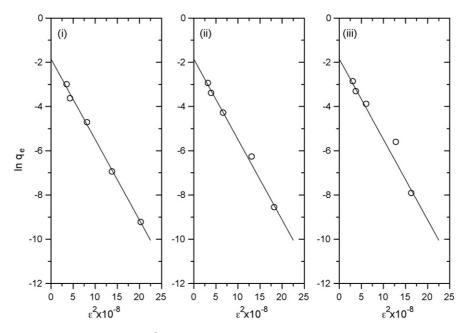

Fig. 5. Dubinin–Radushkevich isotherm plots for Ba^{2+} adsorption on NZVI at different adsorbent doses: (i) 100 mg, (ii) 50 mg, and (iii) 25 mg.

Table 3
Values of the thermodynamic parameters obtained at different concentrations

Initial conc. (M)	ΔH° (kJ/mol)	ΔG° (kJ/mol)		ΔS° (J/(mol K))	
		298	328	298	328
1×10^{-3}	−31.8	−11.4	−9.4	−68.5	−68.5
1×10^{-4}	−43.9	−16.9	−14.2	−91.5	−90.5
1×10^{-5}	−47.1	−20.0	−17.2	−91.1	−91.1
1×10^{-6}	−47.4	−22.2	−19.7	−84.4	−84.4
Average ± S.D.	−42.5 ± 7.3	−16.5 ± 4.8	−14.2 ± 4.3	−87.6 ± 10.5	−86.3 ± 10.5

obtained curve is extrapolated to very low concentrations, the value of ΔH_{id}° came out to be −47.5 kJ/mol. As reported in one of our previous studies [21], since the observed ΔH° values intuitively include the contribution of 'intrinsic' enthalpy change, ΔH_{int}° (always exothermic) and the partial contribution of the dehydration enthalpy of the sorbate cation, ΔH_{dehyd}° (always endothermic), one would expect ΔH_{int}° to have values greater in magnitude than the observed values of ΔH°.

Gibbs energy of adsorption was calculated at each concentration using the corresponding R_d values at both temperatures. The obtained results are given in Table 3. These values are indicative that the adsorption reaction is preferentially driven towards the products, but that this tendency decreases with increasing temperature.

The observed entropy values of adsorption were calculated using those of ΔH° and ΔG° as given in Eq. (10). The negative values given in Table 3 imply that more order is generated as a result of Ba^{2+} adsorption. In such cases, the adsorption process is enthalpy driven. Apart from the adsorbent effects, this behavior is generally expected for ions that have low hydration energies; i.e. those possessing large ionic radius and/or low oxidation states.

3.4. Some comments on adsorption mechanism

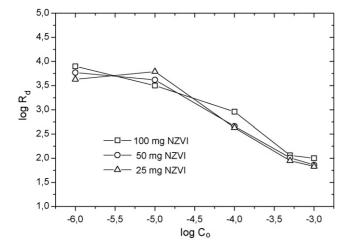Iron nanoparticles are widely accepted to possess a core–shell structure, with the core being composed of Fe^0 while the shell is composed of iron oxide (e.g. [2,8,11,12,16,23]). The oxide layer is developed as a result of the exposure of NZVI to oxygen. It is proposed that the oxide layer, which is about 3–5 nm thick, protects the core of the particles against further oxidation and provides a means for the transport of mass and charge across it (e.g. [7,8,16]). In addition, it was further reported that the oxide layer consists not only of iron oxide but contains also boron (mostly in its +3 oxidation state), the thing responsible for enhancing the particle resistance against atmospheric attack and thus limiting the oxidation [22]. Alternatively, another study suggested that B present at the outer surface of iron nanoparticles is in the soluble sodium borate form that can be removed by rinsing with water [23].

In light of the proposed structural model for NZVI, the reactivity of the particles can be related with the reducing ability of the Fe^0, in addition to the contribution of FeOOH groups as a result of the hydroxylation of the particle surface in aqueous media [2]. The standard electrode potential (SEP) of Ba^{2+} (=−2.91 V, 298 K) is much smaller than that of Fe^{2+} (=−0.44 V, 298 K), hence a redox reaction leading to formation of Ba^0 seems to be highly unlikely. In a recent study in which HRXPS was applied, the mechanism of adsorption on iron nanoparticles was studied for a number of metal ions [12]. According to this study, ions with SEP smaller than that of Fe^{2+} (as it is the case with Ba^{2+}, Zn^{2+}, and Cd^{2+}) did not undergo changes in their valence state upon fixation on NZVI surface. Based on this, it is suggested that such ions are plausibly fixed by FeOOH groups on the surface of iron nanoparticles through electrostatic interactions and/or surface complexation.

More work is needed to reveal a clearer picture of the mechanism of Ba^{2+} adsorption by NZVI.

4. Conclusion

Iron nanoparticles employed in this study consisted mainly of zero-valent iron. Massive oxidation of these particles to γ-Fe_2O_3, Fe_3O_4, and γ-FeOOH phases occurred at the end of adsorption. The kinetic data was best described by pseudo-second-order rate equation. Equilibrium partitioning of Ba^{2+} ions adequately obeyed Freundlich and Dubinin–Radushkevich isotherm models. According to the observed thermodynamic parameters, the adsorption process is exothermic with negative entropy change thus indicating that enthalpy effects form the driving force for adsorption. Further consideration is still required to elucidate other aspects of the adsorption process including the operating mechanism(s).

Fig. 6. Variation of the distribution ratios with the initial concentrations at different adsorbent doses.

References

[1] D.W. Blowes, C.J. Ptacek, S.G. Benner, W.T. McRae Che, T.A. Bennett, R.W. Puls, Treatment of inorganic contaminants using permeable reactive barriers, J. Contam. Hydrol. 45 (2000) 123–137.

[2] Y. Sun, X. Li, J. Cao, W. Zhang, H.P. Wang, Characterization of zero-valent iron nanoparticles, Adv. Colloid Interf. Sci. 120 (2006) 47–56.

[3] S.M. Ponder, J.G. Darab, T.E. Mallouk, Remediation of Cr(VI) and Pb(II) aqueous solutions using nanoscale zero-valent iron, Environ. Sci. Technol. 34 (2000) 2564–2569.

[4] Y. Liu, S.A. Majetich, R.D. Tilton, D.S. Sholl, G.V. Lowry, TCE dechlorination rates, pathways, and efficiency of nanoscale iron particles with different properties, Environ. Sci. Technol. 39 (2005) 1338–1345.

[5] S.H. Joo, A.J. Feitz, D.L. Sedlak, T.D. Waite, Quantification of the oxidizing capacity of nanoparticulate zero-valent iron, Environ. Sci. Technol. 39 (2005) 1263–1268.

[6] X.Q. Li, D.G. Brown, W.X. Zhang, Stabilization of biosolids with nanoscale zero-valent iron (nZVI), J. Nanoparticle Res. 9 (2007) 233–243.

[7] S.R. Kanel, B. Manning, L. Charlet, H. Choi, Removal of arsenic(III) from groundwater by nanoscale zero-valent iron, Environ. Sci. Technol. 39 (2005) 1291–1298.

[8] S.R. Kanel, J.M. Greneche, H. Choi, Arsenic(V) removal from groundwater using nano scale zero-valent iron as a colloidal reactive barrier material, Environ. Sci. Technol. 40 (2006) 2045–2050.

[9] A.B.M. Giasuddin, S.R. Kanel, H. Choi, Adsorption of humic acid onto nanoscale zerovalent iron and its effect on arsenic removal, Environ. Sci. Technol. 41 (2007) 2022–2027.

[10] J. Cao, W-x. Zhang, Stabilization of chromium ore processing residue (COPR) with nanoscale iron particles, J. Hazard. Mater. 132 (2006) 213–219.

[11] X.q. Li, W.-x. Zhang, Iron nanoparticles: the core–shell structure and unique properties for Ni(II) sequestration, Langmuir 22 (2006) 4638–4642.

[12] X.-q. Li, W.-x. Zhang, Sequestration of metal cations with zerovalent iron nanoparticles—a study with high resolution X-ray photoelectron spectroscopy (HR-XPS), J. Phys. Chem. C 111 (2007) 6939–6946.

[13] H.N. Erten, H. Gokturk, Sorption–desorption behavior of barium on clays, J. Environ. Radioactiv. 11 (1990) 183–188.

[14] W. Wang, Z.-h. Jin, T.-l. Li, H. Zhang, S. Gao, Preparation of spherical iron nanoclusters in ethanol–water solution for nitrate removal, Chemosphere 65 (2006) 1396–1404.

[15] K. Sohn, S.W. Kang, S. Ahn, M. Woo, S.K. Yang, Fe(0) nanoparticles for nitrate reduction: stability, reactivity, and transformation, Environ. Sci. Technol. 40 (2006) 5514–5519.

[16] L. Li, M. Fan, R.C. Brown, J.V. Leeuwen, J. Wang, W. Wang, Y. Song, P. Zhang, Synthesis, properties, and environmental applications of nanoscale iron-based materials: a review, Crit. Rev. Environ. Sci. Technol. 36 (2006) 405–431.

[17] R. Han, R. Zou, Z. Zhang, J. Shi, J. Yang, Removal of copper(II) and lead(II) from aqueous solution by manganese oxide coated sand. I. Characterization and kinetic study, J. Hazard. Mater. 137 (2006) 384–395.

[18] S. Azizian, Kinetic models of sorption: a theoretical analysis, J. Colloid Interf. Sci. 276 (2004) 47–52.

[19] Y.S. Ho, G. Mckay, The kinetics of sorption of divalent metal ions onto sphagnum moss peat, Water Res. 34 (2000) 736–742.

[20] S. Kundu, A.K. Gupta, Arsenic adsorption onto iron oxide-coated cement (IOCC): regression analysis of equilibrium data with several isotherm models and their optimization, Chem. Eng. J. 122 (2006) 93–106.

[21] T. Shahwan, H.N. Erten, S. Unugur, A characterization study of some aspects of the adsorption of aqueous Co^{2+} ions on a natural bentonite clay, J. Colloid Interf. Sci. 300 (2006) 447–452.

[22] S.M. Ponder, J.G. Darab, J. Bucher, D. Caulder, L. Craig, L. Davis, N. Edelstein, W. Lukens, H. Nitsche, L. Rao, D.K. Shuh, T.E. Mallouk, Surface chemistry and electrochemistry of supported zerovalent iron nanoparticles in the remediation of aqueous metal contaminants, Chem. Mater. 13 (2001) 479–486.

[23] J.T. Nurmi, P.G. Tratnyek, V. Sarathy, D.R. Bear, J.E. Amonette, K. Peacher, C. Wang, J.C. Linehan, D.W. Matson, R.L. Penn, M.D. Driessen, Characterization and properties of metallic iron nanoparticles: spectroscopy, electrochemistry, and kinetics, Environ. Sci. Technol. 39 (2005) 1221.